

PRECIPITATION EFFECTS FOR KA-BAND SAR

Andreas Danklmayer(1), Madhu Chandra(2)

⁽¹⁾*German Aerospace Center, DLR, Microwaves and Radar Institute,
Oberpfaffenhofen, PO Box 1116, D - 82230 Wessling, Germany,
Email: Andreas.Danklmayer@dlr.de*

⁽²⁾*Chemnitz University of Technology, Dept. of Microwave Engineering and Photonics
Reichenhainerstr. 70, D-09126 Chemnitz, Germany
E-mail: Madhu.Chandra@etit.tu-chemnitz.de*

ABSTRACT

Space-borne Synthetic Aperture Radar (SAR) imaging is often considered to possess both day/night and all weather operational capabilities. Whereas the first argument is true since we are dealing with an active sensor; the second does not hold in cases for which the operating frequencies are above ~ 3 GHz. Indeed, the SAR performance can be significantly affected by atmospheric effects (losses), especially at unfavourable weather conditions. The principal reasons for the restriction on the use of these higher frequencies can be found in clear air losses (water vapour and oxygen), cloud attenuation and attenuation due to precipitation, primarily rain. The scope of this paper covers the activities performed for an ESA-study (Danklmayer, 2009 [1]) under Task 1 (Survey on Precipitation Effects for SAR) and Task 2, the quantitative assessment of the propagation effects and the associated modelling. For the Ka-band rain rates of 10 mm/h are capable to produce visible artefacts. Depending on the climatic region on Earth, the availability of the investigated Ka-band system will vary. Assuming a 5 dB acceptance of the attenuation due to rain, which corresponds to 2 mm/h at 30° incidence angle for the modelled rain cell, the availability will be better than 98% for the European regions and better than 95% for rain-forest in Brazil. Finally, measures and possibilities are suggested, how to mitigate propagation effects in SAR images, together with an outlook on remaining issues to be addressed in future studies.

Keywords: Synthetic Aperture Radar (SAR), microwave imaging, propagation effects, tropospheric effects, rain attenuation, Ka-band

TROPOSPHERIC EFFECTS

The troposphere, as the lowest part of the Earth's atmosphere, reaches from the surface to approximately 12 km above ground and causes, amongst other effects, attenuation of traversing signals due to hydrometeors (rain, snow, hail), atmospheric gases, fog and clouds [2]–[5]. Except at low elevation angles, the attenuation of frequencies below 1 GHz is negligible. Insignificant contributions to the attenuation will be obtained for frequencies up to 10 GHz due to fog and non-precipitating clouds. However the transmission spectrum exhibits peaks for frequencies around 22 GHz and 60 GHz due to molecular resonances from gases i.e. water vapour and oxygen. Whereas absorption effects due to atmospheric gases are present constantly and everywhere, attenuation due to condensed water in the form of precipitation, clouds and fog is infrequent and is limited to certain areas. Attenuation consists of two physical processes: the reduction of the wave's energy due to the heating of the water particles and, the scattering of energy away from the main direction of propagation. Further details on the assessment of atmospheric effects on SAR images can be found in Danklmayer et. al. [7].

MODELLING OF THE ATTENUATION AND BACKSCATTERING EFFECTS IN SAR IMAGES

For the modelling of the attenuation and backscattering effects in SAR images, Fig. 1 and Fig. 2 is clarifying the underlying geometry [7]. The diagram provided at the bottom of Fig. 1 shows the qualitative variation of the normalised radar cross section (NRCS) due to the idealised rain cell. The detailed modelling and calculation is provided in the following two sections.

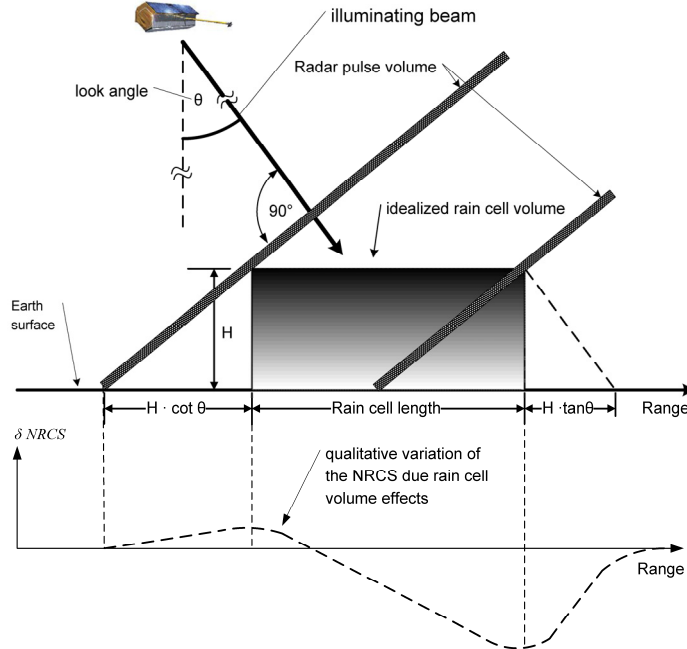


Fig. 1. A depiction of a SAR imaging scenario of an idealised rain cell. In the diagram the qualitative variation of the NRCS due to the rain cell volume effects is given. A combination of backscattering and attenuation can occur, where qualitatively the backscattering due to rain is the minor effect and attenuation the major, [6].

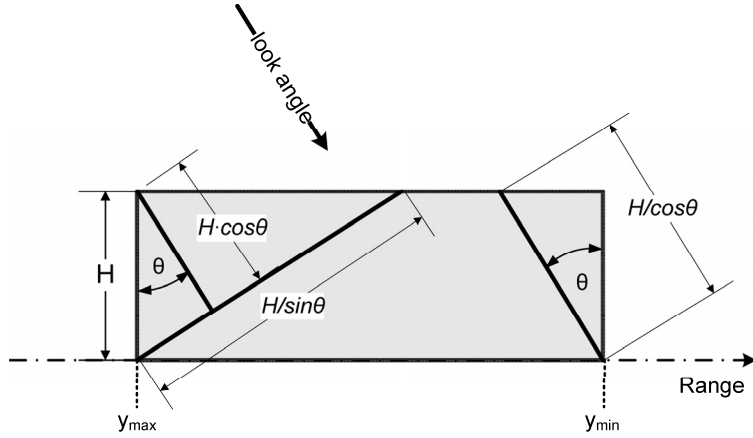


Fig. 2. Geometry of an idealized rain used for quantitative analysis of the attenuation effects, [6].

MODELLING OF THE ATTENUATION UNDER RAIN CONDITIONS FOR X- AND KA-BAND SAR:

For the calculations of the rain rate to cause visible attenuation in X-band and Ka-band SAR images, a simple model illustrated in Fig. 2 (Mehlsheimer, 1998, [6]), is used. A reasonable rain height of 4 km is assumed, as well as a homogenous rain rate for the modelled cell. The incidence angle of the propagating signals was chosen 30°. With the help of (1) and by using the regression coefficients in Table 1, the specific attenuation was calculated. These values are given in Table 2. Finally, the values for the two-way path attenuation for different rain rates (5, 50 and 100 mm/hr) can be found in Table 3. As known from several measurements with existing radar systems, like TerraSAR-X, a total two-way attenuation of 25 dB becomes visible in SAR images in X-band. Thus, it is plausible to estimate the rain rate, which causes such attenuation for Ka-band (35 GHz) frequencies. To this end, the following set of equations is applied

$$\kappa(x, t) = a \cdot R^b \quad (1)$$

where $\kappa(x, t)$ is the specific attenuation in units of dB/km and a and b are the regression coefficients provided in Table 1. R denotes the rain rate in mm/hr.

Table 1. Regression coefficients for estimation of the rain attenuation in Eq. 1

Frequency	Drop size Distribution (DSD)			
	Marshall Palmer		Joss Thunderstorm	
	a	b	a	b
X – band (10 GHz)	0.0136	1.15	0.0169	1.076
Ka- band (35 GHz)	0.268	1.007	0.372	0.783

Table 2. Rain rate [mm/hr] and specific attenuation [dB/km] for the X- and Ka-band frequencies

Rain intensity [mm/hr]	Specific Attenuation [dB/km]	
	X-band @10 GHz	Ka-band @35 GHz
5	0.08	1.31
50	1.22	7.95
100	2.4	13.69

By inserting the total two-way attenuation A(t) for a rain cell of 4 km height with homogeneous rain rate the specific attenuation can be calculated according to the following term

$$\kappa(t) = \frac{A(t)}{2 \cdot \frac{H}{\cos(\theta)}} \quad [\text{dB/km}] \quad (2)$$

Then, the rain rate is found using (1) with the according parameters a and b for Ka-band.

$$R = \sqrt[b]{\frac{\kappa(t)}{a}} \quad [\text{mm/hr}] \quad (3)$$

First calculations using the parameters of the idealised rain cell of 4 km, and 25 dB of total two-way attenuation A(t), assuming the Marshall-Palmer Parameters for Ka-band attenuation results in a rain rate close to 10 mm/hr. This simplified model example demonstrates that such rain rates are fully capable to distort Ka-band SAR measurements. In Fig. 3 the range of values for attenuation and rain rate are extended and the diagram shows the two-way attenuation versus the rain rate for different incidence angle at Ka-band. Similar information is provided for X-band frequencies in Fig. 4. The rain rate which causes 25 dB for the two-way attenuation is much higher, i.e. about 100 mm/hr for the same incidence angle of 30°.

The afore mentioned simple assumptions of a homogenous rain cell with constant precipitation may be somehow optimistic, since a melting layer precipitation may increase the total path attenuation. The melting layer is not yet a very well understood scattering object (Matrosov, 2008, [9]), thus, at present time, modelling would only be possible using strong simplifications and thus this issue offers potential for further research.

Table 3. Maximum attenuation for modelled rain cell shown in Figure 9 [dB]

Rain rate [mm/hr]	Attenuation [dB]	
	10 GHz	35 GHz
5	0.739	12.1
50	11.26	73.43
100	22.17	126.46

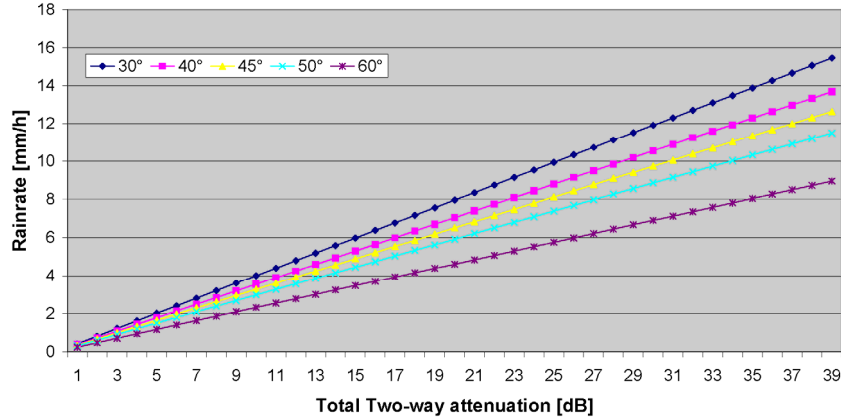


Fig. 3. A diagram of the total two-way path attenuation and the corresponding rain rate for the modelled layer of 4 km height at Ka-band (35 GHz), for different look angles.

In Table 4 the values of the two-way attenuation (Ka-band) for the modelled rain cell as a function of the rain-rates and look angles are tabulated. In addition, Table 5 provides the rain-rates versus the corresponding two-way attenuation (Ka-band) for the incidence angles 30, 40, 45, 50, and 60 degree according to the modelled rain cell of 4 km height.

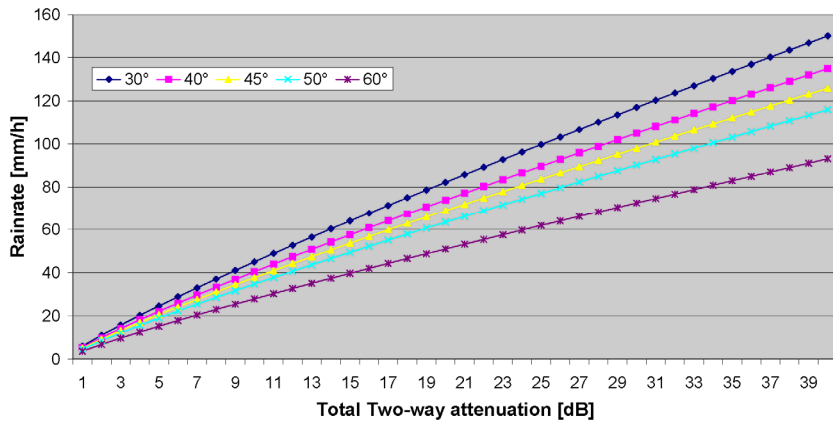


Fig. 4. A diagram of the total two-way path attenuation and the corresponding rain rate for the modelled layer of 4 km height at X-band (10 GHz), for five different look angles.

COMPARISON OF EXPERIMENTAL SAR DATA WITH WEATHER-RADAR DATA AND EXTRAPOLATION OF EFFECTS TO KA-BAND FREQUENCIES

Fig. 5 shows a comparison of two different types of images measured almost at the same time, where the image on the left hand side was acquired with TerraSAR-X strip-map mode in ascending orbit over New York. The image on the right hand side displays the corresponding weather radar image measured by a ground-based weather radar (WSR-88D) located in New York (Nexrad code: KOKX). The data was obtained using the freely available Java NEXRAD viewer provided by NOAA (National Oceanic and Atmospheric Administration), US.

A good agreement between visible artefacts shown in the SAR image (some of them encircled in red colour) and the reflectivity plot on the right hand side was observed. Such reflectivity maps display the echo intensity of the transmitted radar signals and are shown in dBZ. These maps are used to detect precipitation and evaluate storm structures. It is the best available means to compare precipitation volumes and precipitation induced signatures in SAR images. The reason lies in the high achievable spatial resolution and the possibility to measure at almost the same instant of time. The red regions in the weather radar image correspond to reflectivities up to 50, in some cases 55 dBZ, which corresponds to high precipitation intensities typically occurring during thunderstorms.

The comparison of ground based weather radar and SAR data is essential in the process of modelling and estimation of rain intensity information based on SAR (Danklmayer et. al., 2009, [7]).

Table 4. The values of the two-way attenuation (Ka-band) for the modelled rain cell of 4 km height with the rain-rates for the corresponding look angles

Two-way Attenuation [dB]	Rain-rate R [mm/hr] as a function of incidence angle θ [$^\circ$]				
	30°	40°	45°	50°	60°
1	0,41	0,36	0,33	0,30	0,24
2	0,81	0,72	0,66	0,60	0,47
3	1,21	1,07	0,99	0,90	0,70
4	1,61	1,43	1,32	1,20	0,93
5	2,01	1,78	1,64	1,49	1,16
6	2,41	2,13	1,97	1,79	1,40
7	2,81	2,49	2,30	2,09	1,63
8	3,21	2,84	2,62	2,38	1,86
9	3,60	3,19	2,95	2,68	2,09
10	4,00	3,54	3,27	2,98	2,32
15	5,98	5,30	4,98	4,45	3,47
20	7,96	7,05	6,51	5,92	4,61
25	9,94	8,80	8,13	7,39	5,76

Table 5. The rain-rates and the corresponding two-way attenuation (Ka-band) for the look angles 30, 40, 45, 50, and 60 degree according to the modelled rain cell of 4 km height.

Rain rate [mm/hr]	Two-way attenuation [dB] at different incidence angles θ [$^\circ$]				
	30°	40°	45°	50°	60°
1	2,48	2,80	3,03	3,34	4,29
2	4,98	5,62	6,09	6,70	8,62
3	7,48	8,46	9,17	10,08	12,96
4	10,00	11,30	12,25	13,47	17,32
5	12,52	14,15	15,33	16,87	21,68
6	15,04	17,00	18,42	20,27	26,05
7	17,57	19,86	21,52	23,67	30,43
8	20,10	22,72	24,61	27,08	34,81
9	22,63	25,58	27,71	30,48	39,19
10	25,16	28,44	30,81	33,90	43,58

Another test case close to New Orleans, US is provided in Fig. 6 and was selected to perform a comparison between two different types of measurements (left: TerraSAR-X; middle: NOAA ground-based weather radar data) and one artificially generated product (right) based on the modeling approach in this paper. The two almost isolated rain cells with reflectivities of up to 50 dBZ, depicted in the weatherradar image (middle), are ideally suited to be used for extrapolation and modeling of respective attenuation and backscattering effects for Ka-band. As expected, the attenuation due to rain increases dramatically at Ka-band and therefore the visible artefacts are more pronounced but limited to regions where the rain rate is about 10 mm/hr. The backscattering at Ka-band due to rain is also increased compared to X-band which results in zones of bright veils appearing to the left of the precipitation cells (in the direction towards the radar).

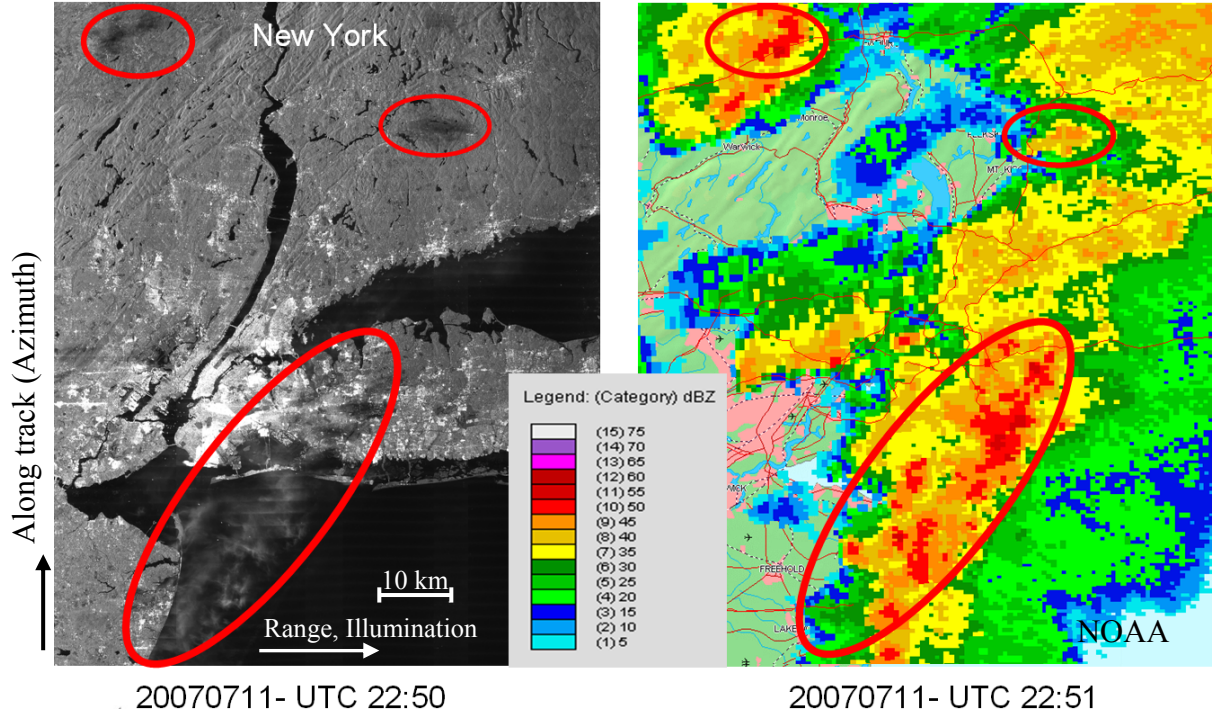


Fig. 5. A test-case showing a comparison of TerraSAR-X and weatherradar data acquired nearly simultaneously (within the same minute) over New York, US. A good agreement between the rain-cell signatures in the SAR-image (left) and the weatherradar image (right) can be observed. The effects are most pronounced for reflectivities of up to 50 dBZ. The SAR-image was acquired in ascending orbit direction and the range direction corresponds with the horizontal. The look direction was from left to right. The vertical corresponds to the along-track direction. Image dimensions are approx. 130 km in azimuth and 100 km in range direction.

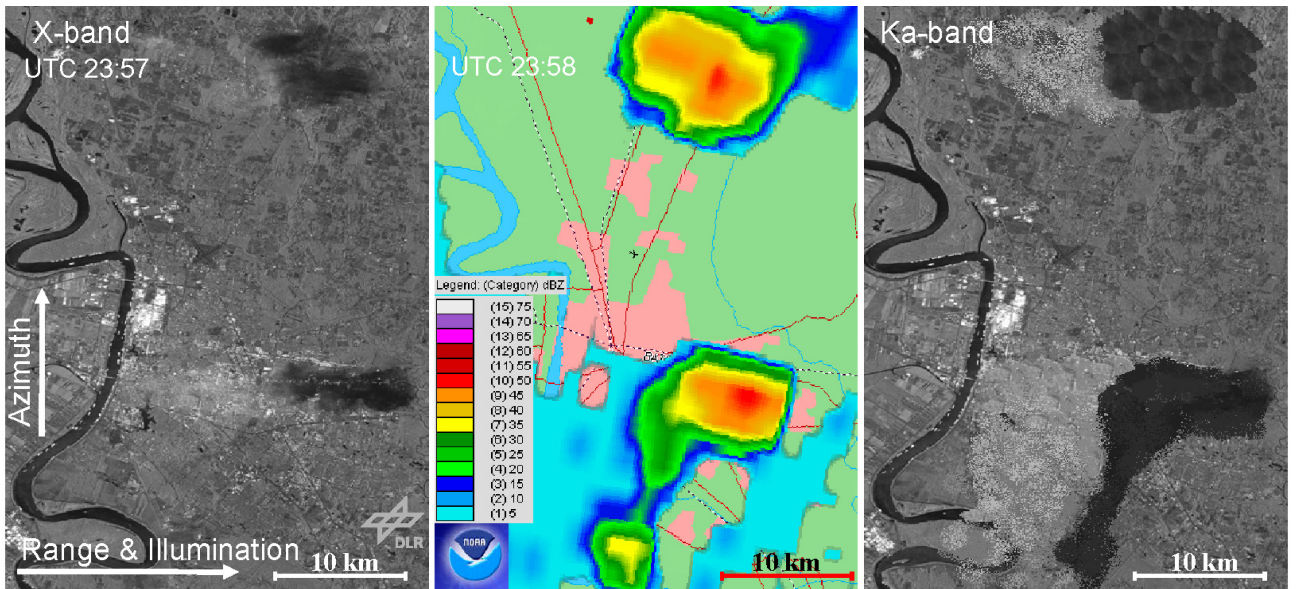


Fig. 6. A test case showing a comparison of three different types of data sets. In the middle a weather radar image is given, showing a reflectivity map of two almost isolated rain-cells with reflectivity values up to 50 dBZ. To the left a corresponding SAR image measured with TerraSAR-X is provided. Signatures due to precipitation can be easily identified. What is shown on the right hand side, is an artificially generated image based on TerraSAR-X data and illustrates how rain introduced artefacts may look like at Ka-band frequencies. The estimation of the attenuation is based on the modelling presented in this paper.

IDENTIFICATION OF MEASURES AND RECOMMENDATIONS TO COUNTERACT AND/OR ENHANCE PRECIPITATION EFFECTS ON SAR

In this section we briefly highlight some of the possibilities to overcome the limitations of the SAR system under investigation due to adverse meteorological conditions. The ideal strategy to identify rain induced signatures would be a multi-frequency SAR system, because attenuation through rain is wavelength dependent. Since the Ka-band SAR under investigation is not equipped with such a multi-frequency sensor set, other ways have to be taken into consideration. Wherever available, ground based weather radar would assist in the process to identify precipitation induced distortions in SAR images. However, world-wide coverage of ground based weather radars is limited to industrialized regions such as the USA or parts of Europe. Especially over the oceanic regions no ground based weather radar data are available and so it is for the polar regions of the Earth. One simple measure to avoid or mitigate precipitation effects are multi-temporal acquisitions over the same scene, since the statistical probability for rain is rather low, as already shown before. As the look angle determines the path length of the propagation path through the precipitation media, steep look angles would reduce the attenuation due to rain, and conversely shallow look angles cause increased values of attenuation (cf. Table 5). The question to what extent scan-on-receive techniques are capable to improve, respectively enhance precipitation effects was addressed by d'Addio and Ludwig (2008) [10], and deserves further consideration. A mitigation of the backscattering can be obtained. However the attenuation will still be present for transmit and receive patterns as is depicted in Fig. 7.

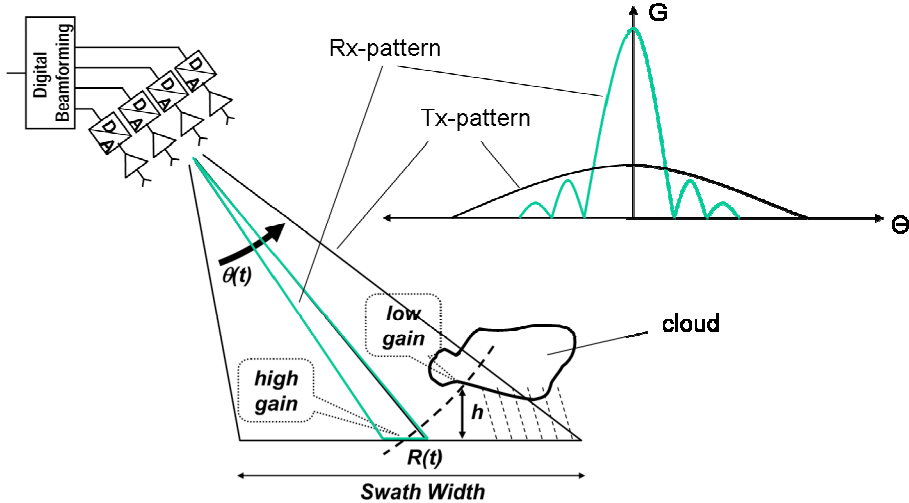


Fig. 7. A depiction of an imaging scenario with Scan-on-receive technique. The different gain in receive Rx (pencil beam) and Tx allows for an improvement of the SNR in the presence of rain for backscattering. However, the attenuation can not be avoided.

CONCLUSIONS AND OUTLOOK

It has been found that attenuation due to rain is the dominating effect, together with backscattering from precipitation for higher frequency bands such as X- and Ka-band. Since the effects of backscattering and attenuation is interconnected to each other it is sufficient to consider at least the major disturbance (=attenuation through rain) in order to flag an affected SAR image. A model to quantify propagation effects in SAR images has been presented, which allows for a quantitative assessment of the pertinent effects. Depending on the climatic region on Earth, the availability of the investigated Ka-band system will vary. Assuming a 5 dB acceptance of the attenuation due to rain, which corresponds to 2 mm/hr at 30° incidence angle for the modelled rain cell used in this paper, the availability will be better than 98% for the European regions and better than 95% for rain-forest in Brazil.

REFERENCES

- [1] A. Danklmayer, Precipitation Effects for Ka-band SAR, ESA-ESTEC/ Final Report Contract No. 21876/08/NL/ST/al, 2009
- [2] Specific Attenuation Model for Rain for Use in Prediction Methods, 2005. ITU-Recommendation P. 838-3.
- [3] M. P. Hall, Effects of the Troposphere on radio communication, IEE, 1979.

- [4] A.W. Doerry, "Atmospheric loss considerations for synthetic aperture radar design and operation," in Proceedings of SPIE, 2004.
- [5] T. Oguchi, "Electromagnetic Wave Propagation and Scattering in Rain and Other Hydrometeors," Proceedings of the IEEE,, vol. 9, pp. 1029–1079, Sepember 1983.
- [6] C. Melsheimer, Signaturen von Regen in Radaraufnahmen des Meeres. Aachen: Shaker Verlag, 1998.
- [7] A. Danklmayer, B. J. Döring, M. Schwerdt, and M. Chandra, Assessment of Atmospheric Propagation Effects in SAR Images, IEEE Transactions on Geoscience and Remote Sensing, vol. 47, No. 10, October 2009, p 3507-3518
- [8] A. Danklmayer, M. Chandra, Comparison of Precipitation effects in X- and Ka-band SAR, IEEE International Symposium on Geosciences and Remote Sensing, Cape Town, ZA, 2009
- [9] S. Y., Matrosov, "Assessment of Radar Signal Attenuation Caused by the Melting Hydrometeor Layer, IEEE Transactions on Geoscience and Remote Sensing, Vol. 46, No. 4, 2008
- [10] D'Addio, S.; Ludwig, M.; Rain Impact on Sensitivity of Ka-band Scan-on-Receive Synthetic Aperture Radars, IEEEInternational Geoscience and Remote Sensing Symposium, (IGARSS) 2008. Volume 3, 7-11 July 2008
Page(s):III - 1174 - III – 1177, Boston, US